Optical separation of heterogeneous size distributions of microparticles on silicon nitride strip waveguides

Saara A. Khan,[1,*] Yu Shi,[1] Chia-Ming Chang,[2] Catherine Jan,[1] Shanhui Fan,[1] Audrey K. Ellerbee,[1] and Olav Solgaard[1]

[1]*Stanford University, Department of Electrical Engineering, Stanford, California 94305, USA*
[2]*Bell Labs, Alcatel-Lucent, 791 Holmdel Road, Holmdel, New Jersey 07733, USA*
[*]*saarak@stanford.edu*

Abstract: We demonstrate two complementary optical separation techniques of dielectric particles on the surface of silicon nitride waveguides. Glass particles ranging from 2 μm to 10 μm in diameter are separated at guided powers below 40 mW. The effects of optical, viscous, and frictional forces on the particles are modeled and experimentally shown to enable separation. Particle interactions are investigated and shown to decrease measured particle velocity without interfering with the overall particle separation distribution. The demonstrated separation techniques have the potential to be integrated with microfluidic structures for cell sorting.

OCIS codes: (130.0130) Integrated optics; (170.4520) Optical confinement and manipulation; (230.7380) Waveguides, channeled.

References and links

1. A. Ashkin, "Acceleration and trapping of particles by radiation pressure," Phys. Rev. Lett. **24**(4), 156–159 (1970).
2. S. C. Chapin, V. Germain, and E. R. Dufresne, "Automated trapping, assembly, and sorting with holographic optical tweezers," Opt. Express **14**(26), 13095–13100 (2006).
3. K. Visscher, S. P. Gross, and S. M. Block, "Construction of multiple-beam optical traps with nanometer-resolution position sensing," IEEE J. Sel. Top. Quantum Electron. **2**(4), 1066–1076 (1996).
4. P. Jákl, A. V. Arzola, M. Šiler, L. Chvátal, K. Volke-Sepúlveda, and P. Zemánek, "Optical sorting of nonspherical and living microobjects in moving interference structures," Opt. Express **22**(24), 29746–29760 (2014).
5. M. P. MacDonald, G. C. Spalding, and K. Dholakia, "Microfluidic sorting in an optical lattice," Nature **426**(6965), 421–424 (2003).
6. I. Ricárdez-Vargas, P. Rodríguez-Montero, R. Ramos-García, and K. Volke-Sepúlveda, "Modulated optical sieve for sorting of polydisperse microparticles," Appl. Phys. Lett. **88**(12), 121116 (2006).
7. A. A. S. Bhagat, H. Bow, H. W. Hou, S. J. Tan, J. Han, and C. T. Lim, "Microfluidics for cell separation," Med. Biol. Eng. Comput. **48**(10), 999–1014 (2010).
8. H. Y. Jaising and O. G. Hellesø, "Radiation forces on a Mie particle in the evanescent field of an optical waveguide," Opt. Commun. **246**(4–6), 373–383 (2005).
9. S. Gaugiran, S. Gétin, J. Fedeli, G. Colas, A. Fuchs, F. Chatelain, and J. Dérouard, "Optical manipulation of microparticles and cells on silicon nitride waveguides," Opt. Express **13**(18), 6956–6963 (2005).
10. K. Grujic, O. Hellesø, J. Hole, and J. Wilkinson, "Sorting of polystyrene microspheres using a Y-branched optical waveguide," Opt. Express **13**(1), 1–7 (2005).
11. K. D. Leake, B. S. Phillips, T. D. Yuzvinsky, A. R. Hawkins, and H. Schmidt, "Optical particle sorting on an optofluidic chip," Opt. Express **21**(26), 32605–32610 (2013).
12. S. Lin and K. B. Crozier, "An integrated microparticle sorting system based on near-field optical forces and a structural perturbation," Opt. Express **20**(4), 3367–3374 (2012).
13. B. S. Ahluwalia, O. G. Hellesø, A. Z. Subramanian, J. S. Wilkinson, J. Chen, and X. Chen, "Integrated platform based on high refractive index contrast waveguide for optical guiding and sorting," Proc. SPIE **7613**, 76130R (2010).
14. B. S. Schmidt, A. H. Yang, D. Erickson, and M. Lipson, "Optofluidic trapping and transport on solid core waveguides within a microfluidic device," Opt. Express **15**(22), 14322–14334 (2007).

#233441 - $15.00 USD Received 29 Jan 2015; revised 19 Mar 2015; accepted 21 Mar 2015; published 30 Mar 2015

15. K. Grujic, O. G. Hellesø, J. S. Wilkinson, and J. P. Hole, "Optical propulsion of microspheres along a channel waveguide produced by Cs+ ion-exchange in glass," Opt. Commun. **239**(4–6), 227–235 (2004).
16. H. Cai and A. W. Poon, "Optical trapping of microparticles using silicon nitride waveguide junctions and tapered-waveguide junctions on an optofluidic chip," Lab Chip **12**(19), 3803–3809 (2012).
17. J. Wang and A. W. Poon, "Unfolding a design rule for microparticle buffering and dropping in microring-resonator-based add-drop devices," Lab Chip **14**(8), 1426–1436 (2014).
18. L. P. Faucheux and A. J. Libchaber, "Confined brownian motion," Phys. Rev. E Stat. Phys. Plasmas Fluids Relat. Interdiscip. Topics **49**(6), 5158–5163 (1994).
19. R. Fuchs, T. Weinhart, J. Meyer, H. Zhuang, T. Staedler, X. Jiang, and S. Luding, "Rolling, sliding & torsion of micron-sized silica particles: experimental, numerical and theoretical analysis," Granul. Matter **16**(3), 281–297 (2014).
20. T. L. Cail and M. F. Hochella, Jr., "Experimentally derived sticking efficiencies of microparticles using atomic force microscopy," Environ. Sci. Technol. **39**(4), 1011–1017 (2005).
21. J. S. Punrath and D. R. Heldman, "Mechanisms of small particle re-entrainment from flat surfaces," J. Aerosol Sci. **3**(6), 429–440 (1972).
22. B. Chu, *Laser Light Scattering* (Academic Press, 1974).
23. A. Subramanian, P. Neutens, A. Dhakal, R. Jansen, T. Claes, X. Rottenberg, F. Peyskens, S. Selvaraja, P. Helin, B. DuBois, K. Leyssens, S. Severi, P. Deshpande, R. Baets, and P. Van Dorpe, "Low-loss singlemode PECVD silicon nitride photonic wire waveguides for 532–900 nm wavelength window fabricated within a CMOS pilot line," IEEE Photon. J. **5**(6), 2202809 (2013).

1. Introduction

The first demonstration of optical trapping with a laser beam (laser tweezers) by Ashkin in 1970 opened the door to studies and applications in a variety of fields [1]. One important application of laser tweezers is label-free particle sorting, which is critical for several biological and clinical applications. However, a laser tweezer has limited ability to sort particles because of its inherent constraint of trapping one particle at a time. While systems have been developed to trap multiple particles using dynamic tweezers [2] or collections of tweezers operating simultaneously [3], such systems are complicated and do not easily scale to large numbers of particles. Optical methods using interference fields have been able to demonstrate increased optical sorting throughput compared to optical tweezers and work primarily with the operation of spatial light modulators for periodic fringes [4–6].

Recently, recognition that the evanescent fields in waveguides can produce sufficient forces to trap and propel particles has become of significant interest as a potential means to efficiently sort large numbers of particles. The application of cell sorting is an essential step in many biological assays and is vital for various applications, ranging from disease diagnostics and drug treatment analysis for conducting fundamental studies on cells [7].

The theory of the forces exerted on particles by evanescent fields has been studied in detail [8], and it has been shown that the total force on the particles is directed towards the waveguide and in the forward direction of light propagation [9]. In the past, evanescent fields have been used to sort particles on Y-junction branches [10], ARROW chips [11], and 3-dB optical splitters [12]. These sorting methods can differentiate two groups of particle sizes, but are not designed to sort a variety of sizes at the same time. Other researchers have shown the potential for multiple particle separation directly on a strip waveguide based on size-specific particle propulsion velocities [13,14], and Gruijic observed that single particles show an increase in velocity with particle size [15]. However, these studies have only investigated and demonstrated particle separation at high guided powers (~138-275 mW) on isolated particles (i.e. 100-μm separation between each particle) to avoid deleterious effects of particle interaction.

The high refractive index contrast in silicon nitride waveguides, compared to waveguides created by potassium or cesium ion exchange, leads to a faster evanescent wave decay; which leads to larger gradients of the evanescent field and exhibits high optical forces on microparticles [9]. The refractive index contrast (Δn ~0.52 as compared to Δn ~0.12 for silicon oxide waveguides in water) enables waveguides of sub-micron thickness (~200-nm). These thin waveguides create large evanescent fields outside of the waveguide for particle propulsion and allows for operation at low guided powers. Recent papers on silicon nitride

#233441 - $15.00 USD Received 29 Jan 2015; revised 19 Mar 2015; accepted 21 Mar 2015; published 30 Mar 2015

waveguides for particle manipulation have investigated microparticle transportation processes using microring-resonators and tapered-waveguide junctions, but have yet to show optical separation by size [16, 17].

In this paper, we demonstrate two complimentary optical separation methods with the use of silicon nitride strip waveguides at significantly lower guided powers than has been previously demonstrated for a mixture of heterogeneous particle sizes (i.e. below 40 mW). The first regime of optical separation, which we term threshold velocity particle separation (<30 mW), operates by propelling small particles (2 μm and/or 4 μm) while leaving large particles (8 μm and 10 μm) stationary. In the second regime of optical separation, which we term terminal velocity particle separation (>30 mW), all the particles in the heterogeneous mixture reach terminal velocity; in this case, separation is based on the variation in particle velocity with particle size. Moreover, our results show that particle interactions have a strong effect on particle flow, and that our separation methods function well in the presence of particle interactions. This type of separation via evanescent fields represents an operating regime for label-free, spatial separation of particles by size along the waveguide.

2. Theory and simulation results

When a particle suspended in fluid is propelled by an optical force, it experiences primarily four forces, as summarized in the equation of motion below:

$$m\frac{d^2x}{dt^2} = F_p + F_s + F_D + F_f \tag{1}$$

where m is the particle's mass, F_p is the optical propulsion force from the guided field, F_s is the optical force from the scattered optical fields from the beginning of the waveguide due to non-guided exponentially-decaying modes, F_D is the drag force produced by the fluid, and F_f is the mechanical frictional force between the surface of the particle and the waveguide. Based on this equation of motion, we construct a model to simulate particle trajectories and to investigate particle separation. For each of the forces in the equation of motion, we provide a heuristic analytic representation or a numerical calculation:

The drag force on a spherical particle, F_D, is well documented in literature, and is equal to

$$F_D = -6\pi\eta R v(t) \tag{2}$$

where η is the viscosity of the fluid with Faxen's correction [18], R is the particle radius, and v(t) is the velocity of the particle at time *t*. In the Faxen correction we take the distance from the particle center to the waveguide surface to be the particle radius in addition to 10nm to match COMSOL simulations.

The frictional force, F_f, is represented with the rolling frictional force model [19]. Previous works have investigated rolling friction for micron-sized silicia particles for the measured lateral force equation. We have adapted this model for our case and chosen values for the rolling adhesion force for silicia particles in water [20]. The analytic representation for the rolling friction is given by the following equation:

$$F_{f,rolling} = \mu_{ro}(\beta mg + F_g + h^{ro}) \tag{3}$$

where μ_{ro} is the rolling friction coefficient, β accounts for the buoyancy force of the particle in water, and g is Earth's gravitational constant. The mass of the particle is calculated as $m = \rho_{glass}V = \rho_{glass}(4/3)\pi R^3$, where $\rho_{glass} = 2.5$ g/cm^3. The buoyancy factor was computed as $\beta = ((\rho_{glass}-\rho_{water})/\rho_{glass}) = 0.60$. The values for the coefficient of rolling friction were chosen to match the AFM roughness of the silicon nitride surface and is $\mu_{ro} = 3.5e\text{-}4$ [19]. The optical gradient force, F_g was computed numerically and will be discussed in the next section. The

#233441 - $15.00 USD Received 29 Jan 2015; revised 19 Mar 2015; accepted 21 Mar 2015; published 30 Mar 2015

rolling adhesion force, h^{ro} was chosen for silicia particles in water at a distance of 10 nm from the surface (as simulated in COMSOL) and ranged from 0 to 0.25nN based on particle size [19].

The optical force from the guided power can be computed numerically using COMSOL given the waveguide geometry and particle size. The total force on the particle is composed of a force directed toward the waveguide and forward in the direction of light propagation [9]. These optical forces are called the gradient (F_g) and propulsion force (F_p). In simulations, the 3D waveguide model geometry consisted of a substrate region, a water region, a waveguide strip region and a sphere region shown in Fig. 1. The waveguides themselves were 10 μm wide with a 200-nm thick Si_3N_4 strip deposited on SiO_2. In Fig. 1 the x-direction is in the direction of light propagation, the y-direction is in the direction of the width of the waveguide, and the z-direction is in the direction of waveguide thickness. The simulated particle was placed 10 nm away from the waveguide surface and the length of the waveguide was set to 4 μm. The 10 nm distance was chosen from expected particle collisions leading to surface force detachment [21]. The detachment was approximated to be the distance at which the attractive and repulsive surface forces transition occurs [20]. Simulation times for the different particle sizes varied between 2 and 24 hours depending on the particle size. We used a fine mesh on the waveguide and particle structures and a Maxwell Stress Force Tensor-derived value in COMSOL to calculate the optical force on the particle in the x-direction. The input optical power was 1W and we studied TE polarization because the waveguide has been optimized for this polarization [9]. Table 1 gives a summary of the relationship between optical forces and particle sizes; we were unable to simulate diameters above 4 μm due to limitations in computer memory. It is interesting to note the overall linearity of optical forces with the diameters of the simulated glass particles. In previous papers a similar linear trend can be extracted for particle sizes between 1 and 4μm particle diameters, but it is important to note that this trend is not linear for the entire range of particle sizes [8, 9].

Table 1. Relationship between optical forces and particle diameters from COMSOL simulations

Particle diameter (μm)	Optical propulsion force (pN/W)	Optical gradient force (pN/W)
1.0	11.34	24.6
2.0	31.6	54.6
3.0	56.0	187.4
4.0	81.2	269.2

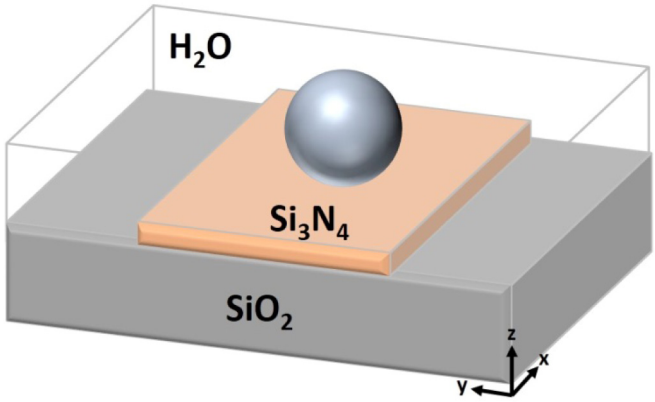

Fig. 1. 3D waveguide simulation geometry for a 10-μm silicon nitride strip waveguide and glass particle submerged in water.

The scattering force at the beginning of the waveguide, F_s, can be approximated from the unguided light from the beginning of the waveguide. The power of unguided light falls off

#233441 - $15.00 USD Received 29 Jan 2015; revised 19 Mar 2015; accepted 21 Mar 2015; published 30 Mar 2015

$1/x^2$, which also results in a scatter force that falls off as $1/x^2$ [22]. Analytically, the scattering force is described as:

$$F_s(x) = \frac{F_{s0}}{(x + x_0)^2} \tag{4}$$

where x_0 is the distance between the beginning of the waveguide to the input laser source, and F_{s0} is used to normalized $F_s(x = 0)$. $F_s(x = 0)$ for each particle size is found from applying the calculated optical force with the unguided light at the coupling interface of the waveguide.

Having the descriptions of the forces experienced by the particle, we can numerically evaluate the equation of motion and obtain the trajectory of particles with different sizes at different guided powers. Four particles with diameters of 1 μm, 2 μm, 3 μm, 4 μm were analyzed, and Fig. 2 displays the trajectories of these particles at guided power levels of 1 mW (a) and 40mW (b). In Fig. 2(a), we see that the large particle get initial momentum from the scattering force and come to a gradual stop, whereas small particles are able to continue their motion down the waveguide. Thus, we can separate smaller particles from larger particles. In Fig. 2(b), however, we observe that at a much higher guided power, all four particles reach terminal velocity and proceed down the waveguide. We define the terminal velocity of a particle to be when the drag and electromagnetic forces on the guide become equal [14]. In this scenario, large particles travel faster than smaller ones, which suggests an alternative mechanism for separation by size. This result is in agreement with other theoretical predictions that the forward velocity of the particle increases with size for high guided powers [8].

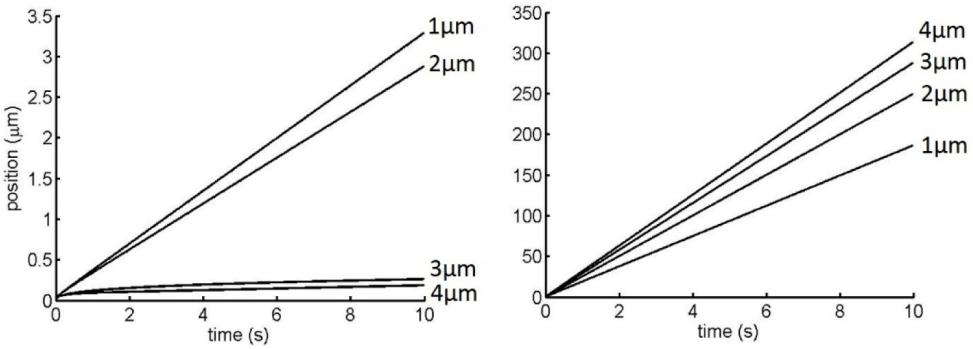

Fig. 2. Particle trajectories at different guided powers. Note the discrepancy in the position of the particles with time between the two separation methods. (a) Particle trajectories at guided power of 1 mW. Smaller particles have enough force to move slowly down the waveguide, while larger particles move a small distance and come to a gradual stop. (b) Particle trajectories at guided power of 40 mW. All particles are moving at terminal velocity down the waveguide and have segregated from largest to smallest along the waveguide based on velocities.

Based on the theoretical model, we propose the existence of two different particle separation mechanisms: threshold velocity separation (<30 mW) and terminal velocity separation (>30 mW). For threshold velocity separation, we expect, at steady state, that small particles travel along the waveguide while the large particles come to a gradual stop, thereby allowing us to separate small particles from larger ones. On the other hand, in terminal velocity separation, large particles travel faster than small particles and reach the end of the waveguide before the smaller particles, which also enables separation.

This predicted motion behavior can be attributed to the effects of the frictional force, F_f. The friction force is dominated by the optical gradient force which increases by particle radius. Therefore, large particles would always experience a larger friction force than smaller

#233441 - $15.00 USD Received 29 Jan 2015; revised 19 Mar 2015; accepted 21 Mar 2015; published 30 Mar 2015

particles. When F_p is small (threshold velocity separation), there exists a region where $F_p > F_f$, for small particles, causing small particles to move, whereas $F_p < F_f$, for large particles, which keeps them stationary. However, under large guided powers (terminal velocity separation), F_p dominates F_f for all particle sizes, in which case F_p dictates the particles' trajectories. Based on the COMSOL results, large particles experience a larger F_p than smaller particles, which explains why large particles move faster than small particles for guided powers > 30 mW.

3. Experimental procedures

We fabricated waveguides on a silicon substrate covered by 2 μm of SiO_2 and ~200 nm of Si_3N_4. SiO_2 was grown by thermal oxidation while Si_3N_4 was deposited by low-pressure chemical vapor deposition and etched into 10 μm-wide waveguides by reactive ion etching. Waveguide film quality in terms of roughness was determined using Atomic Force Microscopy (AFM) on the Si_3N_4 waveguide surface. The RMS roughness of the waveguide was found to be 2.6 nm, which is in accordance with that obtained by others when Si_3N_4 is deposited atop ~2 μm of SiO_2 [23]. Figure 3 shows a 3-D AFM profile of the Si_3N_4 waveguide surface. The strip waveguides were single-mode in the vertical direction and multimode in the horizontal direction. The guide is optimized for TE polarization in the vertical direction to take advantage of the optical forces from the evanescent fields [9].

The experimental setup consisted of a 1550-nm semiconductor laser with a tapered lensed fiber pigtail emitting a 2.5-μm spot coupled into the silicon nitride waveguide at a 14-μm working distance. The propagation loss plus the coupling loss was ~10 dB for a 1-cm long Si_3N_4 waveguide. This loss was found by aligning a single-mode fiber to the output side of the strip waveguide connected to a power meter. The input/output fiber and waveguide were mounted on XYZ translation stages connected to 3-Channel Piezo Controllers (ThorLabs MDT693A) to optimize the coupling.

To test the ability of the waveguide to separate particles of varying sizes, we conducted an experiment in which a heterogeneous mixture of glass particles (size range 2-10 μm) suspended in distilled water was placed on the guide, and we varied the input power from the laser. The suspensions were pipetted onto the waveguide until the entire waveguide was fully covered with liquid. Propulsion of the particles was observed with a CMOS camera and a 50X objective lens (NA = 0.42), which were mounted above the waveguide setup.

The locations of differently sized particles were evaluated from an image of the separated particles by ImageJ, which provided an intensity line scale of the particles along the waveguide. Individual line scans across each particle on the waveguide were used to determine the size of the particles based on the width of their intensity distributions.

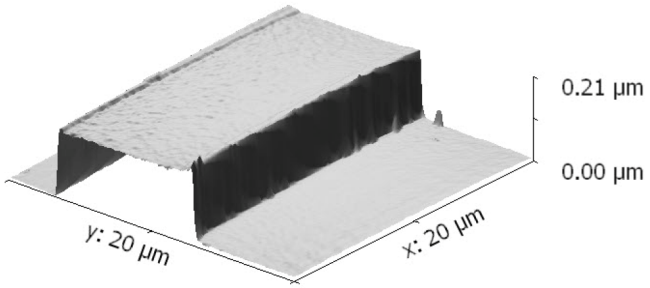

Fig. 3. AFM Image of Si_3N_4 waveguide. RMS roughness is 2.6 on the surface of the waveguide.

#233441 - $15.00 USD Received 29 Jan 2015; revised 19 Mar 2015; accepted 21 Mar 2015; published 30 Mar 2015

4. Experimental results

4.1 Effect of single and multiple particle collisions

Particle collisions are inevitable when attempting to separate particles on strip waveguides. Unlike previous work [15] that dealt only with single-particle propulsion, we investigated the effect of particle interactions on the measured velocity of particles.

We observed that when the waveguide is wide enough to accommodate two different particle sizes (thus the evanescent field can interact with both particles), the particle with the higher velocity may ultimately overtake a downstream particle and collide with it, thus affecting the velocity of both particles. During a collision, we observed that faster particles have the ability to move slightly off the waveguide to bypass slower particles.

We conducted an experiment to investigate particle collisions at a guided power of ~10 mW. At this power, only 2-μm glass particles have the ability to move down the waveguide while all other particle sizes are stationary. We observed collision of a propelling 2-μm glass particle with a stationary 10-μm particle and compared it to the control cases of a 2-μm particle moving unperturbed, as shown in Fig. 4(a). Figure 4(b) shows the trajectory of the 2-μm particle for the two cases. Region A shows the particle trajectory in which the particle collision occurs and region B shows the region in which the particle has overcome the larger particle.

The overall measured average velocities of the 2-μm particle during the 25-s interval of observation were 4.162 μm/sec (no collisions) and 2.787 μm/sec (particle collision) with a linear fit of R^2 = 0.9857 and 0.9735. However, after the collision (region B—15 seconds onwards) the curves again have a similar slope: 4.621 μm/sec (no collisions) and 4.117 μm/sec (particle collision) with a linear fit of R^2 = 0.9926 and 0.9979. This suggests that the particle recovers to the same terminal velocity after the collision, but that particle collisions will change the measured average velocity of a particle over the full length of the strip waveguide. Since the inherent terminal velocity of the particle does not change, particles with larger terminal velocities will overcome slower particles after a collision occurs.

Single and multiple particle collisions between 2-μm and 4-μm particles were also investigated and show that additional collisions decrease the measured velocity further. 2-μm particles were placed and dried on the strip waveguide to ensure they would not move during the experiment. We conducted the experiment at a guided power of 11 mW to stay well below the threshold for the larger particle propagation and at the start of 4-μm particle propagation. Figure 5(a) and 5(b) shows single and multiple particle collisions between 4-um particles with stationary 2-um beads. The overall measured velocity of the 4-μm particle during the 43-s interval of observation is 0.51 μm/sec (single collisions) and 0.28 μm/sec (multiple collisions) with a linear fit of R^2 = 0.954 and 0.9324. However, observing the particle velocity after a particle collision (region B—25 seconds onwards) shows that the curve has a larger slope: 0.758 μm/sec (single collision) with a linear fit of R^2 = 0.9968. Similar to our results in Fig. 4(b), we observe that particle collisions can change the measured average velocity of a particle due to collisions compared to unperturbed propulsion (region B). We additionally show that increasing the number of collisions lowers the measured average velocity of a particle as seen between Fig. 5(a) and 5(b).

#233441 - $15.00 USD Received 29 Jan 2015; revised 19 Mar 2015; accepted 21 Mar 2015; published 30 Mar 2015

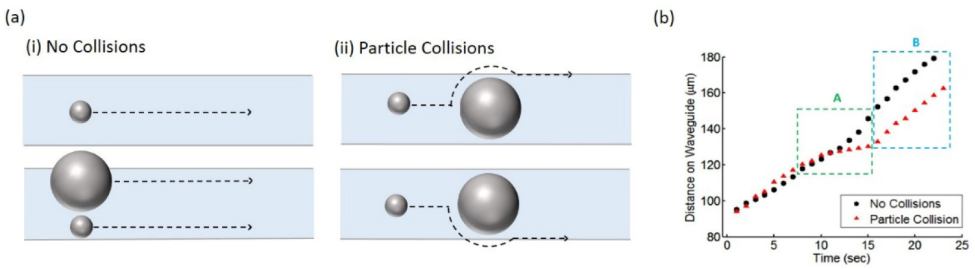

Fig. 4. Effects of single particle collisions

It was also observed that after a 2-μm particle collided with a 10-μm particle it was pushed off the waveguide and was attracted back to the edge of the waveguide. This can be observed from still recordings of a collision instance in Fig. 6. From observing several separate instances of particle collisions it was found that particles smaller than 4 μm could stabilize and travel down the waveguide at different positions along the width of the waveguide. This is likely due to the relative size of the waveguide width compared to the particles and the multimode nature of the waveguide in the y-direction (Fig. 1).

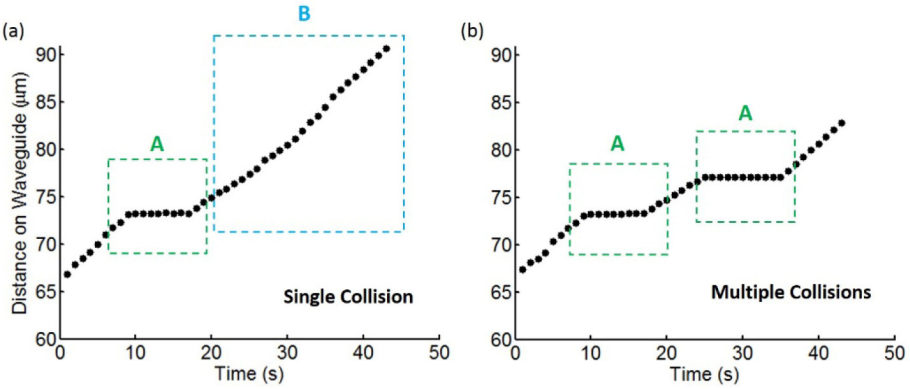

Fig. 5. Effects of single and multiple particle collisions

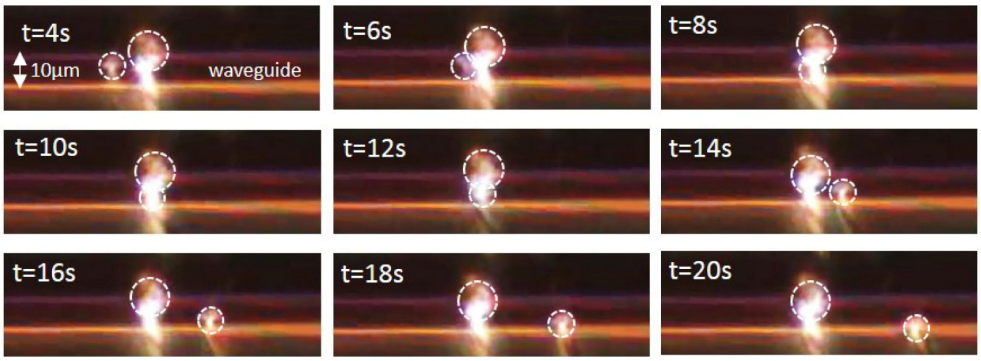

Fig. 6. Representative still recording of a particle collision event. The laser is turned on at time t = 0. The series of pictures documents the interaction between a 10-μm and 2-μm particle at a guided power of 10 mW. The 10-μm particle is stationary while the 2-μm particle is propelled forward by the optical force.

#233441 - $15.00 USD Received 29 Jan 2015; revised 19 Mar 2015; accepted 21 Mar 2015; published 30 Mar 2015

4.2 Distribution of propulsion velocities

Figure 7 shows the measured particle velocities as a function of guided power for a mixed particle suspension containing 2-10-µm glass particles. Each point represents the averaged velocities of four different particles for that size along the waveguide. It should be noted that our results from the previous section suggest that this method of averaging interacting particles to obtain a velocity likely results in lower velocity profiles compared to particles that do not interact with one another. However, in spite of these lower averaged velocities the data shows clearly that velocity is size dependent.

Figure 7 shows the variation in particle velocity versus guided power for several particle sizes. With the upper bound of guided power in our system at 40 mW, we define threshold velocity separation to be at guided powers below 30 mW and terminal velocity separation to be above 30 mW. Note the distinct, particle-specific threshold at which the 4-10-µm particles begin propulsions along the guide. Larger guided powers are required to move larger particles, which ultimately obtain higher propulsion velocities. Threshold guided powers are shown in Fig. 7: at 10 mW, the 2-µm particle experiences enough force to move down the guide; at 11 mW, the 4-µm particle also begins to move; at 13 and 25 mW, we show continued propulsion of the 2- and 4-µm particles since the larger particles do not reach terminal velocity (thus are stationary), and at 38 mW the 8- and 10-µm particles have enough force to propel down the waveguide and all particles on the guide are moving.

From this distribution, we determined that 38 mW is the minimum guided power required for terminal velocity separation of particles based on size, as the particles ordered themselves from largest to smallest as shown in Fig. 7.

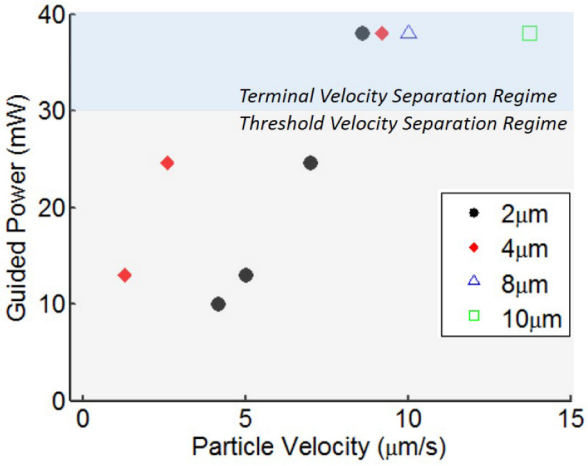

Fig. 7. A heterogeneous mixture of 2-10-µm particles and their terminal velocity at various input powers. At each set of guided powers, particles that are not displayed on the graph are stationary at the beginning of the waveguide.

4.3 Complimentary separation techniques

As shown from Fig. 7 there are two distinct complimentary separation techniques based on the variation of guided power through the silicon nitride waveguide. These two techniques can be utilized for the separation of particles by size. For example, if the user only needs to extract the smallest particles out of a sample then they may operate in the threshold velocity separation regime for their sample set. On the other hand, if the user would like to separate all the particles by size then they can operate in the terminal velocity separation regime.

Threshold velocity particle separation operates with minimal guided powers (<30 mW) and exploits the ability of small particles to move beyond the reach of the scattering force and

#233441 - $15.00 USD Received 29 Jan 2015; revised 19 Mar 2015; accepted 21 Mar 2015; published 30 Mar 2015

reach terminal velocity while larger particles do not. Notably, the larger particles do move specific distances away from the input of the waveguide and then stop as the scattering forces diminish, as detailed in Section 2.

Terminal velocity particle separation can be implemented at higher guided powers (>30 mW). In this regime, all the particles in a heterogeneous mixture (2-10 μm) move down the waveguide. This mechanism allows the system of particles to be spatially separated by size, as the particles move down the waveguide at different velocities. For example, at a guided power of 38 mW, the larger particles were pushed to the front, ahead of the smaller particles. The particles were thus observed to order themselves by size with the largest particles at the front of the line. This result is in line with the predicted behavior described in Section 2, Fig. 2(b).

Figure 8 shows our experimental results of terminal velocity separation. Particles located laterally within a few microns of the waveguide were automatically captured and spatially separated by size. The separated particles were measured 1.5 cm from the waveguide input. Figure 8 shows the breakdown of the relative positions of the particles on the 10-μm wide waveguide. With the exception of one 4-μm particle, all particles are properly ordered and separated according to size within 30 seconds. These results show an 83% separation efficiency for 4-μm particles and a 100% separation efficiency for 2-μm, 8-μm, and 10-μm particles.

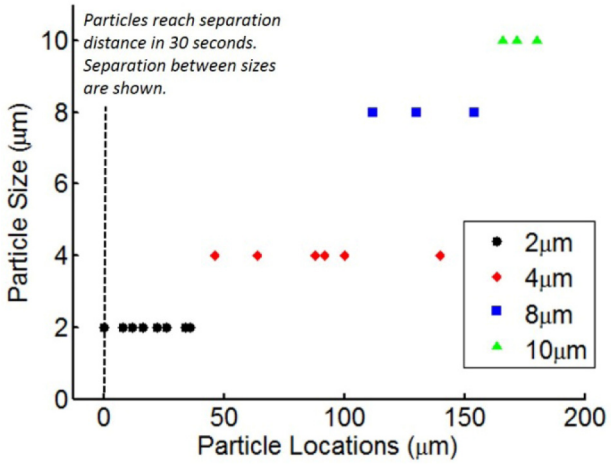

Fig. 8. Distribution of particle separation for glass particles of varying size subject to a guided power of 38 mW. Particles reach separation distance in 30 seconds.

5. Discussion

Our theory predicts the overall observed experimental results, however the experimental results are complicated by particle collisions. It is evident that particle collisions result in lower averaged velocities and each subsequent collision leads to a decrease in measured velocity. To quantify the effects of collisions, we compare theoretical predictions without collisions (Section 2) to experimental results with collisions for 2-μm and 4-μm particle sizes (Section 4) in Fig. 9 and Fig. 10, respectively. Figure 9(a) represents particle velocities for 2-μm and 4-μm particles versus guided powers from our theoretical model in Section 2. A crossover between the 2-μm and 4-μm particle velocities is highlighted in Fig. 9(b), which ultimately causes the 4-μm particle to move faster than the 2-μm particle at guided powers below ~6 mW. A similar crossover and particle dominance between 2-μm and 4-μm particle velocities is seen in the experimental results of Fig. 10(b), albeit at a much higher guided power of ~35 mW. Another difference between the two results is the higher theoretically

#233441 - $15.00 USD Received 29 Jan 2015; revised 19 Mar 2015; accepted 21 Mar 2015; published 30 Mar 2015

predicted velocities (Fig. 9(a)) than are observed experimentally (Fig. 10(b)) for the same guided powers.

The key difference between the theoretical model and the experimental setup is the existence of particle collisions. The theoretical model does not take collisions into account, while our experimental system exhibits multiple particle collisions between different particle sizes. We discussed in Section 4.1 the effect of single and multiple particle collisions on measured velocities. This suggests that the higher crossover point and the lower velocities in the experimental results compared to theoretical simulations are due to particle collisions.

Using ImageJ we monitored the number of collisions that the 2- and 4-um particles experienced and the absolute velocity decrease that occurred from each collision. The decrease in particle velocity from the number of collisions was subtracted from the theoretical velocity results from Fig. 9(a) and plotted in Fig. 10(a). This reveals that once multiple collisions were taken into account in the theoretical results, we were able to find a similar velocity crossover to match experimental results. In future works, we intend on modeling randomized particle collisions due to the particle separation on waveguides to automate the predicted velocity decrease per collision.

Thus, while the collisions lead to a decrease in the measured velocity, the theoretical model and experimental results still agree on the relative velocities between particles. Our theoretical model, which neglects particle interactions, is therefore still useful as it illuminates important phenomena and points to applications of threshold and terminal velocity separation. However, when factoring in the decrease in velocity per collision we obtain an even more robust comparison to experimental values.

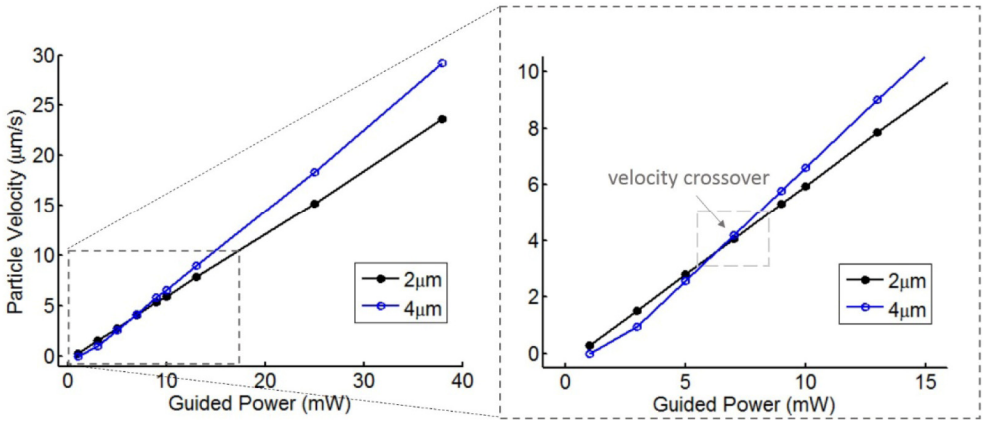

Fig. 9. Theoretical results for 2-μm and 4-μm particle sizes based on force model. Particle interactions were not taken into account.

#233441 - $15.00 USD Received 29 Jan 2015; revised 19 Mar 2015; accepted 21 Mar 2015; published 30 Mar 2015

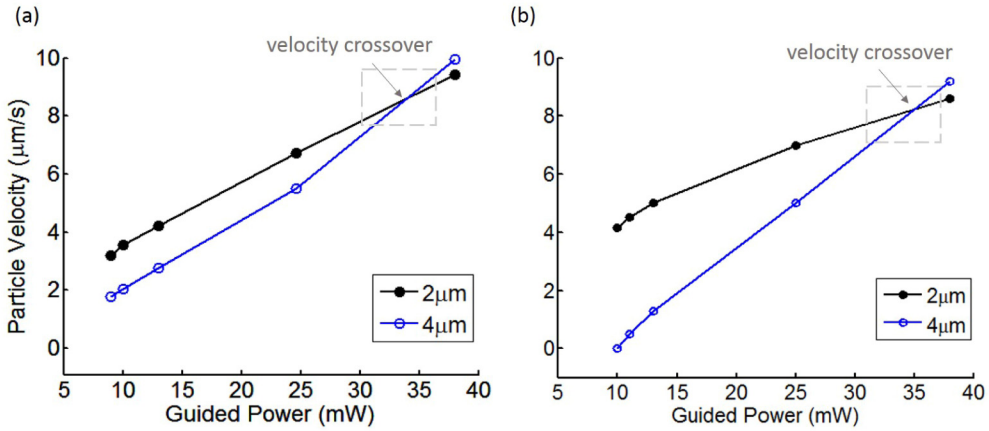

Fig. 10. (a) Theoretical results from Fig. 9 combined with decrease in velocity from multiple particle collisions. (b) Experimental results for 2-μm and 4-μm particles. Particle interactions were present in the system.

6. Conclusion

We demonstrate two complementary strategies for optical separation on silicon nitride waveguides with guided powers below 40 mW. Both techniques can separate a heterogeneous mixture of particles even in the presence of particle interactions. Furthermore, while others have suggested that particle interactions may be a potential issue in particle propulsion [15], we demonstrate that particle interaction leads to lower measured velocities, but does not affect the overall effect of separating particles via the evanescent field.

The threshold particle separation method takes advantage of frictional forces to achieve a binary separation between two groups of particle sizes. This method can be implemented with a single microfluidic channel to input a sample and extract cells out of the end of the guide. In contrast, terminal velocity particle separation relies on differences in relative particle velocities for particle separation. The latter technique has the ability to be integrated with a microfluidic channel for collecting different particle sizes at the output for sorting. Since this technique relies on the relative particle velocities for spatial separation, propagation of different particle sizes along the waveguide will interfere with the separation implementation. A timing technique with microfluidic channels would be required for practical sorting implementations of this technique.

Our paper focuses on separation of a heterogeneous mixture of glass particles of different sizes. Based on other work [9], translating this technique to cells will require an increase in guided powers due to the low refractive index contract between the cells and surrounding medium. However, the methodology and results we provide in this work still hold for different particle types with a shift in guided power required to propel the particles.

In conclusion, threshold and terminal velocity particle separation are demonstrated as optical separation techniques with glass microparticles on silicon nitride strip waveguides and are viable strategies for integrated microfluidic, on-chip sorting.

Acknowledgments

We would like to thank Beth Pruitt, Kristen Lurie, Gennifer Smith, and Evan Scouros for valuable and stimulating conversations. We also thank Antonio Gellineau for help with AFM images. This work was funded by the National Science Foundation Graduate Student Fellowship Program and the Stanford Graduate Fellowship Program.